Title: Spatial map of native duct cell populations in human pancreas and their representation in pancreatic cancers

Short title: Spatial map of human pancreatic (cancer) duct

Van den Bossche JL[1], Van der Vliet M[1], Michiels E[1], Azurmendi Senar O[2], Madran Z[1], Coolens K[1], Van Lint S[1], Nacher M[3], Arsenijevic T[2,4], Messaoudi N[5], Lefesvre P[6], Montanya E[3,7], Rovira M[3], Van Laethem J[2,4], Baldan J[1], Houbracken I[1], Rooman I[1#]

[1]*Vrije Universiteit Brussel (VUB), Translational Oncology Research Center, Laboratory for Medical and Molecular Oncology, Brussels, Belgium*

[2]*Laboratory of Experimental Gastroenterology, Faculty of Medicine, Université Libre de Bruxelles (ULB), Brussels, Belgium*

[3]*CIBER of Diabetes and Associated Metabolic Diseases (CIBERDEM), Hospital Universitari Bellvitge, and Bellvitge Biomedical Research Institute (IDIBELL), Barcelona, Spain*

[4]*Department of Gastroenterology, Hepatology and Digestive Oncology, HUB Bordet Erasme Hospital, Université Libre de Bruxelles, Brussels, Belgium*

[5]*Hepatopancreatobiliaire Heelkunde, Universitair Ziekenhuis Brussel (UZB), Vrije Universiteit Brussel (VUB), Brussels, Belgium*

[6]*Department of Pathology, UZ Brussel, Brussels, Belgium*

[7]*Department of Clinical Sciences, University of Barcelona, Barcelona, Spain*

#Corresponding author: Ilse Rooman, ilse.rooman@vub.be

Grant Support: The work in this study was supported by Fonds Wetenschappelijk Onderzoek (FWO, G0A7322N) and Wetenschappelijk Fonds Willy Gepts (WFWG). IR was awarded a research grant from FWO (Grant ID G0A7322N). J-L VDB is a recipient of a PhD Fellowship of the FWO (Grant ID 11L7724N). EMo acknowledges the support of grant PI22/00334 from Instituto de Salud Carlos III, co-financed by the European Regional Development Fund (ERCF). IH was financially supported by the bequest of Ms. Esther Desmedt and Ms. Irma Noë. SVL was financially supported by the Award Cancer Research - Oncology Center VUB (bequests of Ms. Esther Desmedt and Ms. Irma Noë) and Kom Op Tegen Kanker grant (ANI396). NM is a senior clinical investigator of the FWO (Grant ID 1801425N). JB is supported

by a Foundation Against Cancer Fundamental mandate (2023-038). KC is a recipient of a PhD Fellowship of the FWO (Grant ID 1157221N).

Abbreviations: PDAC= Pancreatic Ductal Adenocarcinoma, ASCP= Adenosquamous Cancer of the Pancreas, NP= Normal human Pancreas, CP= Chronic Pancreatitis, BAS= Basal cell, LUM= Luminal cell.

Correspondence: Ilse Rooman, Laarbeeklaan 103, 1090 Brussels, ilse.rooman@vub.be, +32 24774603

Disclosures: All authors declare no competing interests.

Author contributions: Conceptualization: JL VDB, IR. Data curation: JL VDB, MVDV. Formal analysis: JL VDB, MVDV. Funding acquisition: IR. Investigation: JL VDB, MVDV, EM, OAS, ZM, KC, SVL, PL. Methodology: JL VDB, MVDV. Project administration: JL VDB, IH, IR. Software: MVDV. Resources: MN, NM, EMo. Supervision: TA, MR, JL VL, JB, IH, IR. Writing original draft: JL VDB, IR.

Acknowledgements: The authors thank the Visual and Spatial Tissue Analysis (VSTA) core facility and specifically express their appreciation for the efforts of VSTA technician Emmy De Blay and lab technician Veerle Laurysens. The authors also thank the team at Resolve Biosciences, whose Molecular Cartography® technology was utilized in this study as part of a collaboration.

Abstract

Background & Aims: Epithelial tumors generally resemble the cellular architecture of their tissue of origin. However, this link remains largely unexplored in the pancreas.

Methods: Using Nanostring GeoMx DSP®, Resolve Molecular Cartography® and Nanostring CosMx®, and integration with single cell RNAseq datasets, we mapped the human pancreatic ductal epithelium in non-neoplastic pancreas, and compared it to pancreatic cancer subtypes.

Results: Groups of Keratin-5$^+$ cells among the Pan-Cytokeratin$^+$ cells in the duct have a gene signature reminiscent of stem cells and (supra)basal cells from other tissues. In spatial analysis at single cell resolution, the pancreatic duct manifests as a stratified epithelium comprising a basal and four luminal populations; In large ducts, KRT5$^+$ basal (BAS) cells express ΔNp63 while KRT5$^+$ luminal (LUM)-B cells reside supra-basally and are distinct from the common KRT5$^-$ LUM-A cells. LUM-C and LUM-D cells pertain to intercalated ducts and ductal glands, respectively. LUM-A and -C cells express gel-forming mucins while LUM-B cells have membrane-bound MUC4 and MUC16. In cancer, BAS and LUM-B signatures associate with the basal-like pancreatic ductal adenocarcinoma (PDAC) and correlate with lower survival but exhibit a mixed spatial pattern with a diffracted gene signature. In contrast, adenosquamous cancers of the pancreas (ASCP) preserve the normal spatially unmixed identity of LUM-B cells and BAS cells that is regulated by ΔNp63. Next to ΔNp63, conserved drug targets were identified for both populations.

Conclusion: This study offers a refined pancreatic tumor classification based on the native ductal architecture, with better preservation of the LUM-B and BAS cell population identity in ASCP than in PDAC, including the conserved drug targets.

Keywords: Spatial transcriptomics; adenosquamous cancer; basal cells; heterogeneity.

Introduction

Organs within the human body exhibit a structured organization of specialized epithelial cells that can take on different cell states. With superposition of recurrent meta-programs[1], such as hypoxia or cell

cycle programs, this organization is often retained in tumors reflecting the cell type and states from the tissue of origin. Such relationship has not been studied for the native exocrine pancreas and the pancreatic cancers that arise from it.

The normal exocrine pancreas (NP) comprises acini, responsible for producing digestive enzymes, and ducts that collect and transport these enzymes to the duodenum[2]. Pancreatic Ductal Adenocarcinoma (PDAC), the most prevalent form of pancreatic cancer, consists of tumors with a ductal histology. Next to histological subtyping[3], molecular subclassification of PDAC stems from bulk transcriptomic profiling[4–8] and, more recently, single cell sequencing studies have provided insights with higher resolution[9,10]. A classical and basal-like subtype was discriminated, the latter having poorer prognosis and being characterized by the expression of Keratin-5 (KRT5), Keratin-17 (KRT17) and driven by ΔNp63[11,12], was called 'basal-like' or 'squamous' in reference to other tumors with similar profiles in lung, prostate or breast[13–15]. At single duct and single cell level, transitions of classical and basal-like states were documented[16,17]. Also basaloid, squamoid and mesenchymal states were discriminated, all resorting under the denominator 'basal-like'[9,18]. We reported that ΔNp63 expression in basal-like PDAC is heterogeneous, with not all basal-like tumors or derived cell lines demonstrating ΔNp63 expression[18,19]. Another pancreatic cancer subtype, Adenosquamous Carcinoma of the Pancreas (ASCP), is rare and even more lethal than PDAC[20] and consists of ≥30% ΔNp63$^+$ squamous cells as described in other tissues/cancers[21–23]. Literature suggests that up to 10% of pancreatic tumors can be ASCP, while often diagnosed as PDAC[21,22]. Overlaps or dissimilarities of basal-like PDAC with ASCP beyond the genomic profiles[24,25] are not well documented.

We lack basic insights into the different pancreatic tumor subtypes, mainly basal-like/squamous, and into the pancreatic ductal system that has generally been considered a simple monolayered epithelium of uniform ductal cells. Few studies have reported duct cell heterogeneity based on single cell analyses[26–28]. Our group reported rare ΔNp63$^+$KRT5$^+$ cells situated on the basal lamina of human pancreatic ducts[19]. These KRT5$^+$ cells are more prevalent in chronic pancreatitis (CP), a condition that can predispose to pancreatic cancer[19]. Since pan-cancer studies clearly demonstrated recapitulation

of cell states from the native tissues in many tumors[29–31], we studied the non-neoplastic pancreatic duct cells (NP and CP) and projected these findings to PDAC and ASCP, unveiling a luminal-basal stratification in the native duct system that is best recapitulated in ASCP.

Materials & methods

Human material

Sections from healthy pancreas of multiorgan donors were received from Hospital Universitari Bellvitge-IDIBELL (Barcelona, Spain). Tumor resections were obtained from the Department of Hepatopancreatobiliary Medicine and the Pathology Department of Universitair Ziekenhuis Brussel (UZB). The use of clinical samples conformed with the national guidelines and regulations in Belgium. This study was approved by the ethical committee of UZ Brussel (B.U.N. 1432022000112).

Spatial transcriptomics

NanoString GeoMx Digital Spatial Profiler® (DSP)

GeoMx® (NanoString, Washington, USA) analysis was performed on NP (*n= 1*) and CP (*n= 2*) with pre-identified presence of KRT5^{+} cell regions. Data analysis was performed on the NanoString DSP analysis platform.

Resolve Molecular Cartography (MC)®

The Resolve MC® (Resolve Biosciences, Monheim am Rhein, Germany) study comprised of a custom-designed 100 gene panel (Supplementary Table 1, Supplementary Figure 1) on NP (*n= 3*), CP (*n= 2*) and ASCP (*n= 2*). Transcriptomic PDAC subtype assignment was based on the Chan-Seng-Yue classification[8]. The output files were incorporated into a Seurat object utilizing a customized pipeline developed by adapting publicly available code from GitHub (https://github.com/ostunilab/PDAC_Nature_2023/blob/main/Molecular_Cartography/Nature2023_Human_PDAC_MolecularCartography_analyses.r).

NanoString CosMx® Spatial Molecular Imager

5 µm sections of NP (*n= 1*) and ASCP (*n= 1*) were used for CosMx® analysis (Supplementary Figure 1). The 1000-plex Universal Cell Characterization panel was utilized. Spatial data were processed as above. The Seurat object is utilized as the query object for cell type classification using an integrated reference, with a public single-cell RNA sequencing dataset serving as the reference object (GSE165399, ASCP).

Statistical analysis

The statistical analysis of each experiment is described in the corresponding legend detailing the statistical tests used and sample sizes. Survival analyses were conducted using the survival v3.5-3 and survminer v0.4.9 packages. The log-rank test was used to compare Kaplan-Meier curves and p-values < 0.05 were considered statistically significant. Multivariate Cox proportional hazard regression models, stratified by high and low groups based on GSVA results, were used to analyze survival outcomes, with results presented as hazard ratios (HRs) and 95% confidence interval (CI). Disease free survival (DFS) was defined as the time from diagnosis to the first documentation of recurrent disease following surgery. GraphPad Prism® 10 was used to analyze data. Results are shown as means ± standard deviation.

Results

Human pancreatic KRT5$^+$ cells have a transcriptomic profile consistent with (supra)basal cells from other tissues

We profiled pan-cytokeratin (PanCK)$^+$ KRT5$^-$ and PanCK$^+$ KRT5$^+$ in NP (*n= 1*, 12 ROIs, 3 mm^2) (Supplementary Figure 2A) using NanoString GeoMx®. Comparative transcriptomic analysis demonstrated typical duct cell markers, including *HNF1B* and *ONECUT1/2*, in the KRT5$^-$ population and typical markers of basal cells from other organs, including *KRT15*, *KRT17*, *KRT13*, *TP63*, and *TRIM29*, in the KRT5$^+$ subset of PanCK cells (Figure 1A, Supplementary file 1).

To further substantiate the identity of the KRT5$^+$ cells, we conducted gene set enrichment analysis (GSEA) using the "C8 cell type signature gene sets" (GSEA MSigDB Collections). Top enriched signatures included basal cell types and stem cell types from organs such as lung and esophagus (Figure 1B) and pointed to cells from diverse positions within the epithelial layer (basal/suprabasal) and with distinct activation states (differentiating/proliferating/quiescent). These results hint at a comparable spatial and functional organization of KRT5$^+$ cells within the pancreas. Immunostainings showed KRT5$^+$ cells with expression of ΔNp63 and adjacent KRT5$^+$ without ΔNp63, further supporting basal and suprabasal KRT5$^+$ cells in the pancreas (Supplementary Figure 2B). Comparison of the GeoMx® PanCK$^+$KRT5$^+$ signature with a specific airway and prostate basal cell RNAseq signature[32,33] further confirmed the similarity (Figure 1C).

The differential gene expression between KRT5$^-$ and KRT5$^+$ cells remained consistent in CP (*n= 2*, 8 ROIs, 2 mm^2, Figure 1D). When comparing the KRT5$^+$ cells between NP and CP, stress-response genes (*ATF3, JUN, FOS*) were increased in CP (Figure 1E), suggesting responsiveness to the pathological environment. Interestingly, *Mucin-4* (*MUC4*) was expressed in KRT5$^+$ cells in NP and CP (Figure 1A,D), whereas it was extensively described as undetectable in NP and CP[34–36] and highly expressed in pancreatic cancer[37].

Top differentially expressed genes of KRT5$^+$ cells were annotated in Gene Ontology (Figure 1F); properties included secreted proteins, immune regulation, differentiation, proliferation, and transcriptional regulation.

Collectively, the transcriptomic profiling supported the existence of KRT5$^+$ΔNp63$^+$ pancreatic basal and KRT5$^+$ΔNp63$^-$ suprabasal cells, as reported in lung and prostate.

<u>The human pancreatic duct system is a stratified epithelium with a basal and four luminal populations</u>

Based on the GeoMx® profile above and genes representing ductal cell populations in mouse pancreas[28], we developed a 100-custom gene-panel for single molecule Fluorescence In Situ Hybridization using Resolve Molecular Cartography (MC)®. Since probes for *KRT19* posed risk of optical crowding, *SOX9* was used as a ductal marker, covering small to large ducts[28]. Five cell clusters (clusters 0-4) were subclustered from the *SOX9*$^+$ population (Figure 2A,B). Cluster 0 displayed high *CFTR* (Figure 2C) and mapped to small collecting duct cells in between acini (Figure 2D.c), as in murine pancreas[28]. Clusters 1-3 mapped to large ducts (Figure 2D.a,b) but clusters 1 and 3, having high expression of *KRT5,* were restricted to a confined region, while cluster 2 made up the rest of the duct. Cluster 4 was mainly found in structures consistent with ductal glands, where also cluster 2 cells and to a small extent cluster 0 cells resided (Figure 2D.d).

The (supra)basal cell signature (Figure 1) was confined to clusters 1 and 3, albeit with distinct levels of expression; *TP63* expression was highest in cluster 3, which was positioned at the basal side of cells from cluster 1 that were suprabasal luminal cells (Figure 2D.b). Cluster 3 cells had higher expression of *TP63, KRT15, S100A2, KRT5*, all of which are traditional basal cell markers, as well as higher *AHNAK2, MYC, CSPG4* and *SERPINB5* (Figure 2E). Cluster 1 on the other hand expressed *MUC4, MUC16* and elevated ductal markers *LCN2* and *SOX9* (Figure 2E)[28]. In the spatial plot, cluster 3 *KRT5*$^+$ *KRT15*$^+$ *ΔNp63*$^+$ cells were residing at the basal side of the duct epithelium, while the cluster 1 cells faced the lumen (indicated by asterisk) and expressed *MUC4* (Figure 2F). Immunostainings confirmed transitions from basally located ΔNp63$^+$ cells to ΔNp63$^-$ luminal cells with differential expression of KRT15 and KRT13 (Figure 2G, *n= 3* NP).

Hence, from here on, we called the genuine ΔNp63$^+$ basally positioned cell cluster 3 “BAS” and the cells from cluster 1 “LUM-B” (Luminal-B, with B referring to supra-Basal). Indeed, MUC4$^+$ LUM-B cells were always apically of the BAS cells, being less than 50 microns apart (Figure 2H). Most luminal cells in the duct (cluster 2) are referred to as “LUM-A” (Supplementary Figure 3A-C). Cells from collecting ducts

(cluster 0) are called LUM-C and cells unique to ductal glands are LUM-D (cluster 4). Interestingly, we also detected BAS cells within the ductal glands (Supplementary Figure 3D).

Since we annotated the BAS and LUM-B cells in the human pancreas as 'stem cells' in Figure 1, a comparison was made with suggested 'progenitor' duct cell populations from literature (Supplementary Figure 4); the murine Cluster 7 from Fernandez *et al.*[28] and a subpopulation of cluster 4 from Hendley *et al.*[28] showed expression of *LY6D*, which we identified as a LUM-B marker. The cells defined by Hendley *et al.*[27] also expressed the LUM-B marker *MUC4*. The two suggested human progenitor populations from Qadir *et al.* (cluster 1 and 2)[26] both exhibited expression of the BAS marker *S100A2*. Additional comparison with the human tumor-adjacent ductal populations defined by Moncada *et al.*[38] revealed similarities between their APOL1^{+} hypoxic duct cells and our LUM-B cells, with a trend of higher *MUC4* and *KRT17* expression (not shown).

In conclusion, large pancreatic ducts consist of predominant LUM-A cells while LUM-B cells are confined to regions directly apical of BAS cells. LUM-C cells make up the intercalated ducts and LUM-D cells pertain to ductal glands.

Mucin expression can discriminate the basal and luminal populations

Our analysis revealed distinct mucin expression across the defined clusters (Figure 3A-B, Supplementary Figure 3A); LUM-A was characterized by *MUC5B* expression, with heterogeneous *MUC6* expression. LUM-B expressed *MUC4* and *MUC16*, and *MUC5B* was mutually exclusive with *MUC4* expression. LUM-C only expressed *MUC6*, whereas LUM-D co-expressed *MUC5B* and *MUC6*. The BAS cells showed very limited expression of *MUC4* (Figure 3A).

This mucin RNA expression pattern was validated by immunostainings (Figure 3C-H, *n= 3* NP); LUM-A expressed MUC5B in intra- and interlobular ducts as well as the main pancreatic duct (Figure 3C, Supplementary Figure 3B-C). LUM-B expressed MUC4 (Figure 3D) and MUC16 (Figure 3E). LUM-C, positive for CFTR (Figure 3F), had characteristic MUC6 expression (Figure 3G). Notably, LUM-B had membrane-bound mucins (MUC4, MUC16), whereas LUM-A and LUM-C had gel-forming mucins

(MUC5B, MUC6), suggesting functional differences. LUM-D exhibited expression of both MUC6 and MUC5B (Figure 3H). ΔNp63^{+} (and KRT15^{+}) BAS cells did not express any of the assessed mucins (Figure 3D-E and not shown), neither the MUC4 that showed minor RNA expression, as referred above. These findings, and other suggested markers from Figure 2C (and Supplementary Figure 5) are summarized in Figure 3I as a classification of the different ductal cell types. Apart from co-expression of MUC5B and MUC6, our 100 gene panel did not allow to identify specific markers for LUM-D.

Basal-like PDAC show diffracted Luminal-B and Basal signatures, associated with poor prognosis, and a mixed spatial pattern

The differentiating markers of the basal and luminal cell populations were assessed in a cohort of *n*= 276 treatment-naïve PDAC patients[5]. LUM-D was excluded from the analysis due to the lack of specific markers. Disease-free survival was significantly lower in high expressors of LUM-B and BAS markers (Figure 4A). In contrast, LUM-C markers conferred a better prognosis (Figure 4A). Whereas mutant *KRAS* was consistently detected, using Basescope® assays, in the larger ducts comprising LUM-A and B cells, it was hardly detectable in LUM-C cells of the same tumor (Supplementary Figure 6A). Hence, we concluded that the better survival associated with LUM-C markers was confounded by healthy tissue.

Comparative analysis with previously established bulk transcriptomic subtypes of PDAC[5,8], revealed that the LUM-A and LUM-C profiles are more associated with classical subtypes (Classical-A and Pure Classical), that conferred better prognosis[39], whereas LUM-B and BAS profiles were associated with basal-like subtypes (Basal-Like A and Pure Basal-Like) (Figure 4B) that associated with poorer survival[5,8,39].

To assess how the ductal populations from the native pancreas were represented in cancer, Resolve MC® was used (*n*= 3 PDAC, *n*= 1 ASCP). ASCP cells clustered together in clusters 0 and 1 and the PDAC cells divided into 6 clusters (clusters 2-7) (Figure 4C). Whereas at most one of the LUM-A markers was expressed in the PDAC clusters, they were generally co-expressed in cluster 1 of the ASCP (Figure 4D). A similar observation was made for LUM-B; whereas only one of the markers was expressed in a PDAC

cluster, the ASCP clusters showed co-expression. LUM-C markers were expressed in few clusters in PDAC and completely absent in the ASCP. Notably, co-expression of BAS markers *TP63* and *KRT5* was found in the ASCP cluster 0. The latter BAS population was also the proliferating MKI67^{+} population (Figure 4D). In contrast, PDAC cells were rarely positive for TP63, did not show co-expression of KRT5, and thus did not represent the true BAS cells of the native tissue.

To further investigate this with a broader gene set, scRNA-seq data from *n*= 58 PDAC were used while also integrating an ASCP sample[40] (Figure 4E). Eighteen clusters of tumor cells were defined. The transcriptomic signature of Moffitt *et al.*[7] was used to stratify the tumors into classical and basal-like (Supplementary Figure 6B). In basal-like clusters 9, 13 and 16, the BAS signature indeed appeared diffracted with scattered expression of signature genes in different clusters while the ASCP population (cluster 14) co-expressed the BAS-genes (Figure 4F). This observation was also confirmed in a single nucleus RNAseq dataset containing PDAC and ASCP samples (Hwang *et al.*[9], Supplementary Figure 6C, cluster 5 = ASCP).

At the protein level, the expression of the BAS marker ΔNp63 was not only lower in PDAC (5.9 ± 4.9%, *n*= 6) than in ASCP (52.6 ± 18.6%, *n*= 6) (p-value= 0.0001, Unpaired t-test) (Figure 4G), it was also rarely co-expressed with KRT5 underscoring the diffracted expression of the native BAS markers in PDAC, in contrast to ASCP (Figure 4H, Supplementary Figure 6D). The same observation was made for LUM-B marker MUC4 (8.4 ± 4.4% in *n*= 5 PDAC -one outlier was excluded- compared to 40 ± 21% in *n*= 6 ASCP, p-value= 0.0098, Unpaired t-test, Supplementary Figure 6E).

In summary, PDAC has only a diffracted and spatially mixed representation of the native ductal cell types.

ASCP displays a spatially unmixed pattern of LUM-B and BAS cells consistent with the native tissue

In the ASCP cells from Figure 4C, we identified two distinct populations; cluster 1 exhibited a LUM-B profile, while cluster 0 expressed BAS markers. After subclustering the ASCP cells from the scRNA-seq dataset (Figure 4E), we again obtained two clusters (Figure 5A). Differential gene expression analysis

revealed indeed a BAS (cluster 0) and LUM-B (cluster 1) population (Supplementary Figure 7A). Pathway analysis using the "C2: curated gene sets" from the MSigDB Collection indicated that BAS cells are proliferative, with upregulation of multiple proliferation or cell cycle-associated pathways, metastasis/invasiveness and epithelial-to-mesenchymal transition (Figure 5B) while LUM-B cells were enriched for pathways associated with luminal phenotypes, keratinization and epithelial differentiation.

Using immunostainings (*n*= 6 ASCP), it was observed that the ΔNp63-high expressing BAS cells were preferentially located at the outer rim of the tumor nests, while the MUC4^{+}MUC16^{+} LUM-B cells were in the center (Figure 5C). This was confirmed with Resolve MC® (Supplementary Figure 7B). The proliferation marker KI67^{+} and EMT markers SNAI2 and S100A2 were higher in outer ΔNp63-high regions versus central ΔNp63-low regions (Figure 5C, Supplementary Figure 7C, *n= 6* ASCP). Of the proliferative (KI67^{+}) population within ASCP, 33.48 ± 11 % expressed only ΔNp63, whereas 14.8 ± 10.4 % expressed only MUC4 and 25.8 ± 17 % expressed both (Supplementary Figure 7D, *n* = 6 ASCP). Thus, in total 59 % of the KI67^{+} cells express ΔNp63 in ASCP. In conclusion, we identified a spatial unmixing of BAS and LUM-B in ASCP.

Because of a recent report of squamoid, basaloid and mesenchymal single cell states in pancreatic cancer[9], we performed a targeted assessment using their suggested markers. The basaloid markers overlapped with the ΔNp63-high regions comprising BAS cells while the squamoid markers are congruent with the ΔNp63-low regions comprising LUM-B cells (Supplementary Figure 8-9B).

To further confirm the spatial unmixing, mirroring that of the native tissue, we performed cell type classification using an integrated reference[41], where we first projected the two ASCP subcluster profiles from Figure 5A onto a region of healthy pancreas analyzed by CosMx®. The BAS cluster 0 had a higher prediction score in the TP63^{+} basal cell population of NP (mean= 0.65) compared to the LUM-B cluster 1 (mean= 0.35) (Figure 5D). Similarly, the LUM-B cluster had a higher prediction score in the LUM-B cells (mean= 0.65) than in the basal cells (mean= 0.35). When projecting onto the ASCP tissue, the BAS

profile was enriched at the outer rim of the nests, while the LUM-B profile was in the center (Figure 5E).

In conclusion, ASCP recapitulates the spatially unmixed BAS and LUM-B cells from the native tissue, demonstrating also functional differences.

Potential therapeutic targets: the conserved regulator ΔNp63 or population-specific genes

ΔNp63 is described as a mediator of the basal cell state[11,12,19]. Hence, we first assessed its role as regulator of BAS cell identity. Overexpression of ΔNp63 in normal exocrine-derived human organoids (Figure 6A, Supplementary File 2) induced BAS genes including *TP63, S100A2, KRT17, TFAP2A* (Figure 6B). C8 cell type genesets (MSigDB Collections) showed that transduced organoids indeed associated with basal cells and non-transduced associated with duct cell types (Figure 6C). ΔNp63 is thus sufficient to drive the BAS state in a non-cancer context. Accordingly, knockdown of *ΔNp63* in Human Pancreatic Ductal Epithelial (HPDE) cells, a non-cancerous duct cell line with high expression of ΔNp63 and KRT5[19], induced the LUM-B markers *MUC4* and *MUC16*. Similarly, in cancer, using data of Somerville *et al.* (i.e. shRNA-mediated knockdown of ΔNp63 in the BxPC3 cell line, a squamous cell line with the highest expression of ΔNp63 of pancreatic cancer cell lines[11]), also showed LUM-B markers *MUC4* and *MUC16* upon inhibition of ΔNp63 expression with enrichment for luminal signatures, while the downregulated genes were associated with squamous and basal cell states (Figure 6F). The genes downregulated in HPDE cells with ΔNp63 knockdown were also enriched in BxPC3 cells with high ΔNp63 expression, and vice versa (Figure 6G). This suggests that non-cancer HPDE and the cancer BxPC3 cells share a similar BAS state, and upon ΔNp63 inhibition, both transition to a LUM-B state. Interestingly, when performing such analysis with gene signatures from ASCP (Figure 5A), the ASCP BAS profile is strongly enriched in the BxPC3 WT (wild type cells) while the ASCP LUM-B profile is enriched for the BxPC3 with KD (knockdown) of ΔNp63 (Figure 6H). Overall, inhibition of ΔNp63 thus can drive BAS to LUM-B transition in non-cancerous and cancerous cells.

With treatment strategies to therapeutically target ΔNp63 underway[42,43], we also searched for potentially conserved therapeutic targets specific for the two ASCP populations by comparing data from Figure 5A with those from GeoMx® analysis in Figure 1. We performed a literature search and consulted the Drug Bank for currently available therapies for the BAS and LUM-B specific targets (Figure 6I). Those targets that were represented in the CosMx® panel were validated showing indeed localization in either the BAS or the LUM-B cells in ASCP (Supplementary Figure 9C-D). Whereas they exhibited a scattered expression pattern in PDAC, they were all expressed to some extent in ASCP (Supplementary Figure 9E) underscoring the potential for future combination therapies in ASCP.

Discussion

The pancreatic duct has traditionally been described as a monolayered epithelium. However, in our previous publication[19], we challenged this by demonstrating rare cells located on the basal lamina beneath cells lining the ductal lumen. Leveraging new spatial technologies, we now revealed that the human pancreatic duct comprises four distinct luminal populations and a basal one, each with a unique spatial position and transcriptomic profile.

With GeoMx® analysis, we captured the signature of all KRT5$^+$ cells. It highlighted significant similarities with KRT5$^+$ (supra)basal cells from other organs such as lung and prostate[32,33]. The spatial assessment with Resolve MC® revealed a BAS cell population that is exclusively situated at the basal side of LUM-B cells that on their turn are clearly distinct from the neighboring LUM-A cells. Their signatures remain incompletely defined due to several limitations. These include a lack of specific purification markers, constraints of single-cell and single-nucleus RNA sequencing technologies—such as shallow sequencing depth and inefficiency for rare cell types—and the absence of readily available spatial transcriptomic platforms with full transcriptome resolution at the single cell level. Nevertheless, we identified markers such as mucins, that can help distinguish these cell types. Intriguingly, LUM-B cells express MUC4 and MUC16, both of which have been extensively described not to be present in the healthy pancreas and to be expressed in aggressive pancreatic cancer.

Interestingly, with our more comprehensive analysis, we occasionally observed BAS cells in the ductal glands, which we had not detected earlier[19]. These glands possibly serve as progenitor niches, from which cells migrate to larger ducts following tissue damage[44]. The functional role of BAS cells and their presumed stem cell potential -as suggested by the gene expression analysis- whether residing in large ducts or ductal glands, remains to be determined. The unique localization of LUM-B cells near BAS cells suggests that they could potentially originate from BAS cells. In other organs, basal-to-suprabasal cell transitions have been reported in response to epithelial barrier damage[45,46]. Qadir *et al.*[26] for human pancreas, and Fernandez *et al.*[28] and Hendley *et al*.[27] for mouse pancreas, indicated a subset of cells in the ductal tree with potentially higher regenerative or proliferative capacity. We did not specifically address this here. Yet, *LY6D*, a common marker for the rare Wnt-responsive progenitor-like cells in the murine pancreas[27,28] is a LUM-B cell marker. Indeed, we lack any evidence for BAS cells in the murine pancreatic duct system, as also elaborated in our previous work[19].

We transposed our new insights of the native tissue to pancreatic cancer where there is an urgent need for patient stratification based on tumor biology for allocating treatments. Most progress was made by stratifying PDAC based on a transcriptomic classification into classical and basal-like/squamous tumors. ASCP on the other hand is a rare pancreatic tumor that lacks any specific guidelines and is treated as PDAC[22,23]. Although basal-like/squamous PDAC is named for its transcriptomic similarity to basal or squamous tumors in other organs, our results demonstrate that it is at most “basal-like” with this nomenclature referring now to the NP and underscoring the only diffracted BAS gene signature. In contrast, ASCP has genuine BAS and LUM-B cells, preserving the native identity, with thorough spatial unmixing. For the first time, our study thus offers a classification of pancreatic cancers that aligns with the native tissue, as is the norm for most other cancers. Additionally, our discoveries in the NP helped to finetune our understanding of newly reported cell types/states, such as the squamoid and basaloid cell states, from a recent single-cell study[9]. Of note,

whereas the latter paper referred to these cell states in PDAC, they did also include ASCP in their cohort.

Furthermore, we found that ΔNp63 is a conserved driver of the BAS state and its loss facilitates a BAS-to-LUM-B transition in both non-cancerous and cancerous contexts. Prior attention has gone into therapeutic targeting of ΔNp63[47] with some drugs that could potentially convert the aggressive BAS to the LUM-B cell state[42,43]. In addition, we identified other conserved targets for the BAS cells and added in targets for LUM-B cells envisioning a dual approach where both BAS and LUM-B cells could be attacked. Notably, the differential mucin expressions among the ASCP cell populations are interesting therapeutic targets, e.g. the use of bosutinib (MUC4 inhibitor)[48] and CAR-T cells designed against specific mucins[49]. This warrants further preclinical studies for which recent murine models of ASCP can become very useful[50].

Our findings also raised important questions regarding the cell of origin in pancreatic cancer. Both acinar and ductal cells have been proposed as progenitors of PDAC[2], but our refined classification of the pancreatic ductal system warrants considering subpopulations of duct cells. It remains to be explored whether these different subsets of cells can preferentially give rise to PDAC or to ASCP. It also warrants further investigation if and how differentiation processes presumably occurring in the native tissue (e.g. BAS to LUM-B cells) may apply to tumor plasticity.

In summary, our spatial transcriptomic study of the pancreas resulted in a biologically underpinned nomenclature of pancreatic tumors and sets the stage for future research.

References

1. Gavish, A. *et al.* Hallmarks of transcriptional intratumour heterogeneity across a thousand tumours. *Nature 2023 618:7965* **618**, 598–606 (2023).
2. Backx, E. *et al.* On the Origin of Pancreatic Cancer: Molecular Tumor Subtypes in Perspective of Exocrine Cell Plasticity. *Cell Mol Gastroenterol Hepatol* **13**, 1243 (2022).

3. Verbeke, C. Morphological heterogeneity in ductal adenocarcinoma of the pancreas - Does it matter? *Pancreatology* **16**, 295–301 (2016).

4. Collisson, E. A. *et al.* Subtypes of pancreatic ductal adenocarcinoma and their differing responses to therapy. *Nat Med* **17**, 500–503 (2011).

5. Puleo, F. *et al.* Stratification of Pancreatic Ductal Adenocarcinomas Based on Tumor and Microenvironment Features. *Gastroenterology* **155**, 1999-2013.e3 (2018).

6. Bailey, P. *et al.* Genomic analyses identify molecular subtypes of pancreatic cancer. *Nature* **531**, 47–52 (2016).

7. Moffitt, R. A. *et al.* Virtual microdissection identifies distinct tumor- and stroma-specific subtypes of pancreatic ductal adenocarcinoma. *Nat Genet* **47**, 1168–1178 (2015).

8. Chan-Seng-Yue, M. *et al.* Transcription phenotypes of pancreatic cancer are driven by genomic events during tumor evolution. *Nature Genetics 2020 52:2* **52**, 231–240 (2020).

9. Hwang, W. L. *et al.* Single-nucleus and spatial transcriptome profiling of pancreatic cancer identifies multicellular dynamics associated with neoadjuvant treatment. *Nat Genet* **54**, 1178–1191 (2022).

10. Di Chiaro, P. *et al.* Mapping functional to morphological variation reveals the basis of regional extracellular matrix subversion and nerve invasion in pancreatic cancer. *Cancer Cell* **42**, 662-681.e10 (2024).

11. Somerville, T. D. D. *et al.* TP63-Mediated Enhancer Reprogramming Drives the Squamous Subtype of Pancreatic Ductal Adenocarcinoma. *Cell Rep* **25**, 1741 (2018).

12. Wang, X. *et al.* Identification of a ΔNp63-Dependent Basal-Like A Subtype-Specific Transcribed Enhancer Program (B-STEP) in Aggressive Pancreatic Ductal Adenocarcinoma. *Mol Cancer Res* **21**, 881–891 (2023).

13. Affandi, K. A., Tizen, N. M. S., Mustangin, M. & Zin, R. R. M. p40 Immunohistochemistry Is an Excellent Marker in Primary Lung Squamous Cell Carcinoma. *J Pathol Transl Med* **52**, 283 (2018).

14. Hanna, K. *et al.* Primary prostatic squamous cell carcinoma. *Urol Case Rep* **34**, 101478 (2021).

15. Badowska-Kozakiewicz, A. M. & Budzik, M. P. Immunohistochemical characteristics of basal-like breast cancer. *Contemp Oncol* **20**, 436 (2016).

16. Pitter, K. L. *et al.* Systematic Comparison of Pancreatic Ductal Adenocarcinoma Models Identifies a Conserved Highly Plastic Basal Cell State. *Cancer Res* **82**, 3549–3560 (2022).

17. Raghavan, S. *et al.* Microenvironment drives cell state, plasticity, and drug response in pancreatic cancer. *Cell* **184**, 6119-6137.e26 (2021).

18. Michiels, E. *et al.* High-resolution and quantitative spatial analysis reveal intra-ductal phenotypic and functional diversification in pancreatic cancer. *J Pathol* **262**, 76–89 (2024).

19. Martens, S. *et al.* Discovery and 3D imaging of a novel ΔNp63-expressing basal cell type in human pancreatic ducts with implications in disease. *Gut* **71**, 2030–2042 (2021).

20. Taniwaki, S. *et al.* Sarcomatous Component in Pancreatic Adenosquamous Carcinoma: A Clinicopathological Series of 7 Cases. *Anticancer Res* **39**, 4575–4580 (2019).

21. Del Arco, H., Chakiba-Brugère, C., Salabert, L. & Béchade, D. Adenosquamous Carcinoma of the Pancreas. *Clin Med Insights Oncol* **13**, (2019).

22. Paramythiotis, D. *et al.* Adenosquamous carcinoma of the pancreas: two case reports and review of the literature. *J Med Case Rep* **16**, 395 (2022).

23. Simone, C. G. *et al.* Characteristics and Outcomes of Adenosquamous Carcinoma of the Pancreas. *Gastrointest Cancer Res* **6**, 75 (2013).

24. Hayashi, A. *et al.* A unifying paradigm for transcriptional heterogeneity and squamous features in pancreatic ductal adenocarcinoma. *Nat Cancer* **1**, 59–74 (2020).

25. Braun, R. *et al.* Clinical Outcome and Prognostic Factors of Pancreatic Adenosquamous Carcinoma Compared to Ductal Adenocarcinoma—Results from the German Cancer Registry Group. *Cancers (Basel)* **14**, 3946 (2022).

26. Qadir, M. M. F. *et al.* Single-cell resolution analysis of the human pancreatic ductal progenitor cell niche. *Proc Natl Acad Sci U S A* **117**, 10876–10887 (2020).

27. Hendley, A. M. *et al.* Single-cell transcriptome analysis defines heterogeneity of the murine pancreatic ductal tree. *Elife* **10**, (2021).

28. Fernández, Á. *et al.* A Single-Cell Atlas of the Murine Pancreatic Ductal Tree Identifies Novel Cell Populations With Potential Implications in Pancreas Regeneration and Exocrine Pathogenesis. *Gastroenterology* **167**, 944-960.e15 (2024).

29. Li, H. *et al.* Reference component analysis of single-cell transcriptomes elucidates cellular heterogeneity in human colorectal tumors. *Nat Genet* **49**, 708–718 (2017).

30. Lim, E. *et al.* Aberrant luminal progenitors as the candidate target population for basal tumor development in BRCA1 mutation carriers. *Nat Med* **15**, 907–913 (2009).

31. Van Keymeulen, A. *et al.* Reactivation of multipotency by oncogenic PIK3CA induces breast tumour heterogeneity. *Nature* **525**, 119–123 (2015).

32. Zhang, D. *et al.* Stem cell and neurogenic gene-expression profiles link prostate basal cells to aggressive prostate cancer. *Nat Commun* **7**, (2016).

33. Hackett, N. R. *et al.* The Human Airway Epithelial Basal Cell Transcriptome. *PLoS One* **6**, e18378 (2011).

34. Choudhury, A. *et al.* Human MUC4 Mucin cDNA and Its Variants in Pancreatic Carcinoma. *The Journal of Biochemistry* **128**, 233–243 (2000).

35. Hollingsworth, M. A., Strawhecker, J. M., Caffrey, T. C. & Mack, D. R. Expression of MUC1, MUC2, MUC3 and MUC4 mucin mrnas in human pancreatic and intestinal tumor cell lines. *Int J Cancer* **57**, 198–203 (1994).

36. Balagué, C. *et al.* Altered expression of MUC2, MUC4, and MUC5 mucin genes in pancreas tissues and cancer cell lines. *Gastroenterology* **106**, 1054–1061 (1994).

37. Gautam, S. K. *et al.* MUC4 mucin- a therapeutic target for pancreatic ductal adenocarcinoma. *Expert Opin Ther Targets* **21**, 657 (2017).

38. Moncada, R. *et al.* Integrating microarray-based spatial transcriptomics and single-cell RNA-seq reveals tissue architecture in pancreatic ductal adenocarcinomas. *Nat Biotechnol* **38**, 333–342 (2020).

39. Suurmeijer, J. A. *et al.* Impact of classical and basal-like molecular subtypes on overall survival in resected pancreatic cancer in the SPACIOUS-2 multicentre study. *Br J Surg* **109**, 1150 (2022).

40. Zhao, X. *et al.* Single-cell transcriptomics reveals heterogeneous progression and EGFR activation in pancreatic adenosquamous carcinoma. *Int J Biol Sci* **17**, 2590–2605 (2021).

41. Stuart, T. *et al.* Comprehensive Integration of Single-Cell Data. *Cell* **177**, 1888-1902.e21 (2019).

42. Ramsey, M. R., He, L., Forster, N., Ory, B. & Ellisen, L. W. Physical association of HDAC1 and HDAC2 with p63 mediates transcriptional repression and tumor maintenance in squamous cell carcinoma. *Cancer Res* **71**, 4373–4379 (2011).

43. Fisher, M. L., Balinth, S. & Mills, A. A. ΔNp63α in cancer: Importance and therapeutic opportunities. *Trends Cell Biol* **33**, 280 (2022).

44. Yamaguchi, J. *et al.* Pancreatic duct glands (PDGs) are a progenitor compartment responsible for pancreatic ductal epithelial repair. *Stem Cell Res* **15**, 190–202 (2015).

45. Ruysseveldt, E., Martens, K. & Steelant, B. Airway Basal Cells, Protectors of Epithelial Walls in Health and Respiratory Diseases. *Frontiers in allergy* **2**, (2021).

46. Pitzen, S. P. & Dehm, S. M. Basal epithelial cells in prostate development, tumorigenesis, and cancer progression. *Cell Cycle* **22**, 1303–1318 (2023).

47. Samanta, A., Saha, P., Johnson, O., Bishayee, A. & Sinha, D. Dysregulation of delta Np63 alpha in squamous cell carcinoma and its therapeutic targeting. *Biochimica et Biophysica Acta (BBA) - Reviews on Cancer* **1879**, 189034 (2024).

48. Zhang, C. *et al.* Small molecule inhibitor against onco-mucins disrupts Src/FosL1 axis to enhance gemcitabine efficacy in pancreatic ductal adenocarcinoma. *Cancer Lett* **551**, 215922 (2022).

49. Lin, H. K. *et al.* Muc16CD is a novel CAR T cell target antigen for the treatment of pancreatic cancer. *Molecular Therapy: Oncology* **32**, 200868 (2024).

50. Yang, D. *et al.* Loss of p53 and SMAD4 induces adenosquamous subtype pancreatic cancer in the absence of an oncogenic KRAS mutation. *Cell Rep Med* **5**, 101711 (2024).

51. Chijimatsu, R. *et al.* Establishment of a reference single-cell RNA sequencing dataset for human pancreatic adenocarcinoma. *iScience* **25**, (2022).

52. Peng, S. *et al.* UBE2S as a novel ubiquitinated regulator of p16 and β-catenin to promote bone metastasis of prostate cancer. *Int J Biol Sci* **18**, 3528 (2022).

53. Ruan, S. *et al.* Integrin β4-targeted cancer immunotherapies inhibit tumor growth and decrease metastasis. *Cancer Res* **80**, 771 (2019).

54. Mehraj, U. *et al.* Cryptolepine Targets TOP2A and Inhibits Tumor Cell Proliferation in Breast Cancer Cells - An In vitro and In silico Study. *Anticancer Agents Med Chem* **22**, 3025–3037 (2022).

55. Knox, C. *et al.* DrugBank 6.0: the DrugBank Knowledgebase for 2024. *Nucleic Acids Res* **52**, D1265–D1275 (2024).

56. Nitiss, J. L. Targeting DNA topoisomerase II in cancer chemotherapy. *Nat Rev Cancer* **9**, 338 (2009).

57. Caporali, S. *et al.* Targeting the PTTG1 oncogene impairs proliferation and invasiveness of melanoma cells sensitive or with acquired resistance to the BRAF inhibitor dabrafenib. *Oncotarget* **8**, 113472 (2017).

58. Zhang, L. & Wang, X. Characteristics of long-chain acyl-CoA synthetases in metabolism and cancer. *Clinical and Translational Discovery* **3**, e200 (2023).

59. Santofimia-Castaño, P. *et al.* Targeting the Stress-Induced Protein NUPR1 to Treat Pancreatic Adenocarcinoma. *Cells* **8**, 1453 (2019).

60. Zang, R. *et al.* TMPRSS2 and TMPRSS4 promote SARS-CoV-2 infection of human small intestinal enterocytes. *Sci Immunol* **5**, 3582 (2020).

61. Neumann, T. *et al.* Targeting a cancer-specific LYPD3 glycoform for tumor therapy. *Frontiers in Drug Discovery* **3**, 1298916 (2023).

62. Dorff, T. B. *et al.* PSCA-CAR T cell therapy in metastatic castration-resistant prostate cancer: a phase 1 trial. *Nature Medicine 2024 30:6* **30**, 1636–1644 (2024).

63. Fan, R. *et al.* Tasquinimod suppresses tumor cell growth and bone resorption by targeting immunosuppressive myeloid cells and inhibiting c-MYC expression in multiple myeloma. *J Immunother Cancer* **11**, e005319 (2023).

64. Chung, Y. H. *et al.* Viral nanoparticle vaccines against S100A9 reduce lung tumor seeding and metastasis. *Proc Natl Acad Sci U S A* **120**, e2221859120 (2023).

65. Gautam, S. K. *et al.* MUC4 mucin- a therapeutic target for pancreatic ductal adenocarcinoma. *Expert Opin Ther Targets* **21**, 657 (2017).

Figure Legends

Figure 1: Non-neoplastic human pancreatic KRT5$^+$ cells have a transcriptomic profile consistent with (supra)basal cells from other tissues

(A) Volcano plot of differentially expressed genes between Pan-cytokeratin (PanCK)$^+$ Keratin-5 (KRT5)$^-$ and PanCK$^+$KRT5$^+$ cells in normal human pancreas (NP). Analysis was performed using GeoMx®. Top expressed genes and known basal/duct markers are shown. (B) Gene Set Enrichment Analysis (GSEA) applied to data from panel A with cell type genesets (c8.all.v2024.1.Hs.symbols.gmt). Number of permutations = 1000, normalization performed using meandiv. (C) Enrichment plots using published

profiles[32,33] applied to the genes from panel A (PanCK$^+$KRT5$^+$ cells). NES = 1.17 (airway) and 1.66 (prostate). (D) Volcano plot of PanCK$^+$KRT5$^-$ and PanCK$^+$KRT5$^+$ cells in human chronic pancreatitis (CP) analyzed by GeoMx®. Top expressed genes and known basal and duct markers are shown. (E) Volcano plot of PanCK$^+$KRT5$^+$ cells in NP versus CP. (F) Chord plot of PanCK$^+$KRT5$^+$-specific genes expressed in NP with the associated Gene Ontology Term. The absolute Log_2Fold Change values are represented with a color scheme. For panels A, D and E, statistical analysis was performed with a linear mixed model (LMM) with Benjamini-Hochberg (BH) correction. Genes with p-value < 0.05 were considered differentially expressed.

Figure 2: The non-neoplastic human pancreatic duct system is a stratified epithelium with a basal and four luminal populations

(A) UMAP (Uniform Manifold Approximation and Projection) illustrating *SOX9* expression in all non-neoplastic pancreatic cells from NP and CP samples analyzed by Resolve MC®. (B) Clustered UMAP of the subsetted *SOX9*$^+$ duct populations. (C) Heatmap demonstrating top marker genes for every cluster from panel B using the FindAllMarkers function. Wilcoxon rank sum test was used for statistical analysis with min.diff.pct= 0.2. (D) Spatial plot showing the ductal system by *SOX9* expression and the location of the clusters from panel B. Panels a-d are higher magnification insets of the overview plot. (E) Volcano plot showing differentially expressed genes between the two KRT5$^+$ clusters, i.e. cluster 3 and cluster 1. Parameters for statistical analysis were logfc.treshold = 1, min.pct = 0, p-value < 0.05. (F) Spatial plot of cluster 1 and 3 to illustrate their location and expression of four marker genes (*TP63, KRT5, KRT15, MUC4*). (G) Immunofluorescent staining illustrating basal/suprabasal cells, discriminated by expression of ΔNp63, KRT15 and KRT13. Blue arrows indicate ΔNp63$^+$KRT13$^-$ cells, beige arrows indicate ΔNp63$^-$ KRT13$^+$ cells. (H) MUC4-ΔNp63 proximity analysis, i.e. distance in micrometer of MUC4$^+$ cells to ΔNp63$^+$ cells. (I) Spatial plot same as in panel D a-d while now using the newly proposed basal-luminal cell nomenclature as explained in main text. Asterisk labels lumen of the duct.

Figure 3: Mucin expression can discriminate the basal and luminal populations

(A) UMAPs illustrating the expression of *MUC5B, MUC4, MUC6* and *MUC16* in different duct populations. Cells highlighted in yellow co-express both markers. (B) Spatial plot of different mucins (*MUC5B, MUC4, MUC6*) in NP. (C-H) Immunofluorescent stainings of the different markers used to distinguish luminal and basal populations, namely (C) MUC5B, (D) MUC4, KRT17, ΔNp63, (E) MUC16 and ΔNp63, (F) CFTR and Amylase, (G) MUC6 and Amylase, (H) MUC6 and MUC5B. White arrowheads indicate the different populations. (I) Classification of luminal and basal populations with their specific mucin expression patterns, corresponding location and additional markers. Genes in bold have also been confirmed at the protein level in Figure 3F, Supplementary Figure 2B, Supplementary Figure 5A and Figure 2G. Lumen is indicated by asterisk.

Figure 4: Basal-like PDAC shows diffracted BAS and LUM-B signatures associated with poor prognosis, and a mixed spatial pattern

(A) Kaplan-Meier plots depicting the disease-free survival of a cohort of *n= 276* treatment-naive PDAC patients. Red lines represent patients with high expression of the signature, blue lines represent low expressing patients. Groups were based on median value. Log rank test was used, and statistically significant changes were accepted at p-value < 0.05. (B) Forest plots showing the odds ratio (OR) for luminal and basal signatures in patient groups with specific subtypes of Puleo *et al.*[5] and Chan-Seng-Yue *et al.*[8]. Low and high groups were based on median value. (C) Clustered UMAP of Pancreatic Ductal Adenocarcinoma (PDAC) and Adenosquamous Carcinoma of the Pancreas (ASCP) samples analyzed by Resolve MC® (D) Heatmap showing the different ductal classification markers (LUM-A = *MUC5B* and *LCN2*, LUM-B = *MUC4* and *MUC16*, LUM-C = *MUC6* and *CFTR*, BAS = *TP63* and *KRT5*) and proliferation marker *MKI67*. Wilcoxon rank sum test was used for statistical analysis with min.diff.pct= 0.2. (E) Clustered UMAP of the merged scRNA-seq object of Chijimatsu *et al.*[51] and Zhao *et al.*[40]. (F) Heatmap of selected basal-like PDAC clusters and the ASCP cluster for specific BAS markers (*KRT5, S100A2, KRT17, KRT14, AQP3, KRT15, ITGB4*). Wilcoxon rank sum test was used for statistical analysis with min.diff.pct= 0.2. (G) Quantification of immunofluorescently stained ΔNp63^{+} BAS cells and MUC4^{+}

LUM-B cells in PDAC and ASCP using HALO® image analysis software (Indica Labs, New-Mexico, USA). Data is represented as means with standard deviation. Unpaired t-test was used to determine statistical significance. *p < 0.05, **p < 0.01, ***p < 0.001. *n= 6* PDAC and *n= 6* ASCP. (H) Immunofluorescent stainings of BAS markers ΔNp63 and KRT5 on sections of ASCP (left) and PDAC (right).

Figure 5: ASCP displays a spatially unmixed pattern of LUM-B and BAS cells consistent with the native tissue

(A) Clustered UMAP of subsetted ASCP cells (cluster 14) from Figure 4E. (B) GSEA analysis applied to data from panel A using curated gene sets (c2.all.v2024.1.Hs.symbols.gmt). (C) Immunofluorescent stainings for BAS (ΔNp63, KRT17), LUM-B (MUC4, MUC16), proliferation (MKI67) and epithelial-to-mesenchymal transition (SNAI2) markers in ASCP. (D) Projection of reference cell signatures obtained from the clusters of panel A, i.e. cluster 0/BAS and cluster 1/LUM-B, on sections of NP analyzed by CosMx®, as described in Stuart *et al.*[41]. Statistical significance was determined using an unpaired t-test. *p < 0.05, **p < 0.01, ***p < 0.001, ****p<0.0001. (E) Projection of reference cell signatures obtained from the clusters of panel A (cluster 0/BAS and cluster 1/LUM-B) on sections of ASCP analyzed by CosMx®.

Figure 6: Potential therapeutic targets: the conserved regulator ΔNp63 or population-specific genes

(A) Lentiviral transduction of exocrine-derived organoids in passage 2 for introduction of ΔNp63-mCherry. (B) Volcano plot showing transduced versus control organoids. Genes shown overlap with the GeoMx® data of Figure 1A. Logfc.treshold = 1, min.pct = 0, p-value < 0.05. (C) GSEA analysis applied to data from panel B with cell type genesets (c8.all.v2024.1.Hs.symbols.gmt). (D) Volcano plot showing Human Pancreatic Ductal Epithelial (HPDE) cells with and without knockdown of ΔNp63. Genes shown overlap with the GeoMx® data of Figure 1A. (E) Volcano plot showing BxPC3 cells with versus without knockdown of ΔNp63 obtained from Somerville *et al.*[11]. Genes shown are characteristic BAS and LUM-B markers. (F) GSEA analysis applied to data from panel E using curated gene sets

(c2.all.v2024.1.Hs.symbols.gmt). (G-H) Enrichment plots for the BxPC3 ΔNp63 knockdown data of panel E for (G) HPDE profiles of panel D and of (H) ASCP profiles from Figure 5A. (I) Table of conserved drug targets in BAS and LUM-B populations of ASCP and their currently available targeting strategies[52–65].

Figure 1

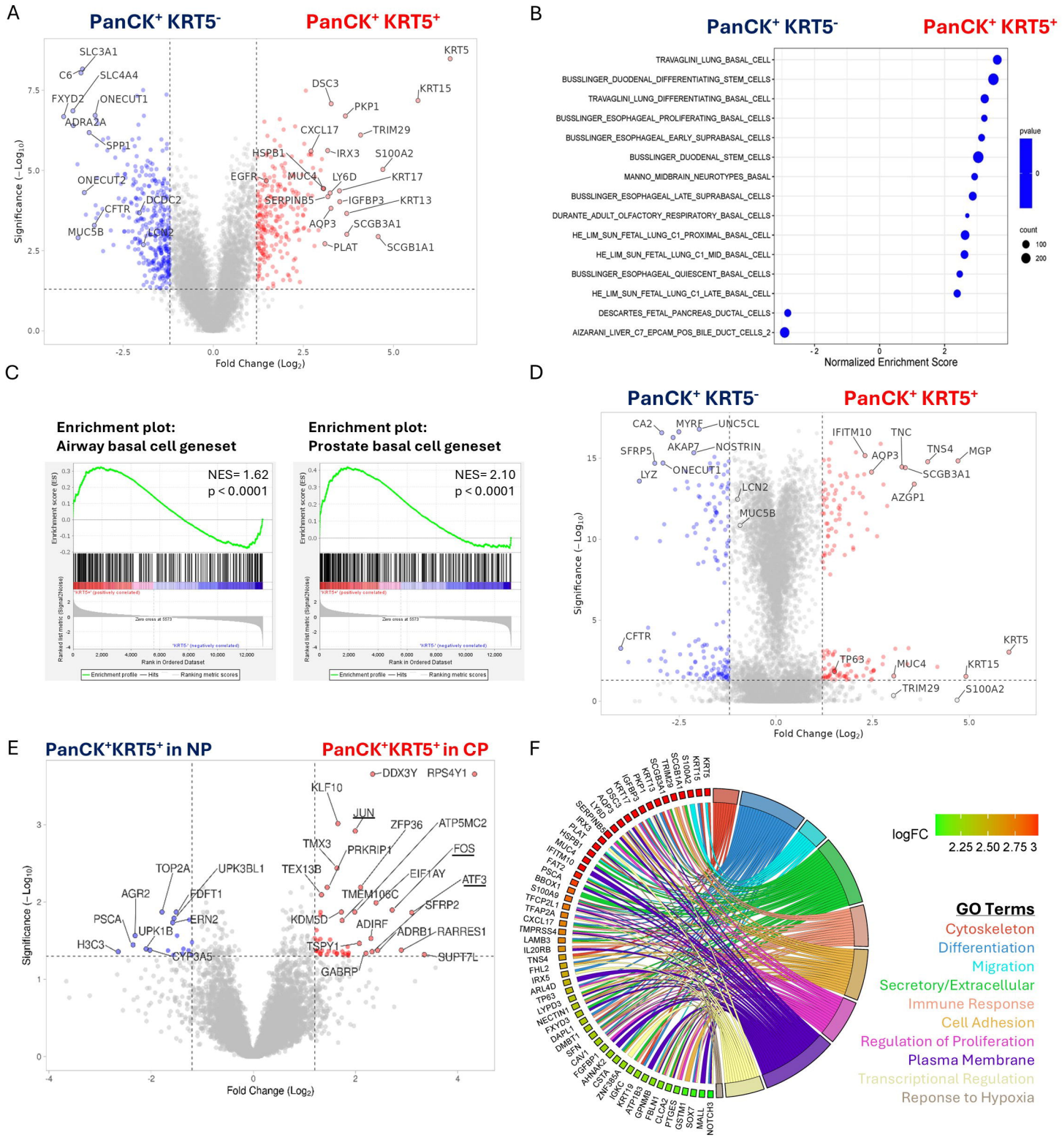
A
PanCK+ KRT5-
PanCK+ KRT5+
SLC3A1
C6
SLC4A4
FXYD2
ONECUT1
ADRA2A
SPP1
ONECUT2
CFTR
DCDC2
MUC5B
LCN2
KRT5
DSC3
KRT15
PKP1
CXCL17
TRIM29
HSPB1
IRX3
S100A2
EGFR
MUC4
LY6D
KRT17
SERPINB5
IGFBP3
KRT13
AQP3
SCGB3A1
PLAT
SCGB1A1
Significance (−Log10)
Fold Change (Log2)
B
PanCK+ KRT5-
PanCK+ KRT5+
TRAVAGLINI_LUNG_BASAL_CELL
BUSSLINGER_DUODENAL_DIFFERENTIATING_STEM_CELLS
TRAVAGLINI_LUNG_DIFFERENTIATING_BASAL_CELL
BUSSLINGER_ESOPHAGEAL_PROLIFERATING_BASAL_CELLS
BUSSLINGER_ESOPHAGEAL_EARLY_SUPRABASAL_CELLS
BUSSLINGER_DUODENAL_STEM_CELLS
MANNO_MIDBRAIN_NEUROTYPES_BASAL
BUSSLINGER_ESOPHAGEAL_LATE_SUPRABASAL_CELLS
DURANTE_ADULT_OLFACTORY_RESPIRATORY_BASAL_CELLS
HE_LIM_SUN_FETAL_LUNG_C1_PROXIMAL_BASAL_CELL
HE_LIM_SUN_FETAL_LUNG_C1_MID_BASAL_CELL
BUSSLINGER_ESOPHAGEAL_QUIESCENT_BASAL_CELLS
HE_LIM_SUN_FETAL_LUNG_C1_LATE_BASAL_CELL
DESCARTES_FETAL_PANCREAS_DUCTAL_CELLS
AIZARANI_LIVER_C7_EPCAM_POS_BILE_DUCT_CELLS_2
pvalue
count
Normalized Enrichment Score
C
Enrichment plot:
Airway basal cell geneset
NES= 1.62
p < 0.0001
Enrichment plot:
Prostate basal cell geneset
NES= 2.10
p < 0.0001
Enrichment score (ES)
Rank in Ordered Dataset
Enrichment profile
Hits
Ranking metric scores
D
PanCK+ KRT5-
PanCK+ KRT5+
CA2
MYRF
UNC5CL
SFRP5
AKAP7
NOSTRIN
LYZ
ONECUT1
LCN2
MUC5B
CFTR
IFITM10
TNC
AQP3
TNS4
MGP
SCGB3A1
AZGP1
KRT5
TP63
MUC4
KRT15
TRIM29
S100A2
Significance (−Log10)
Fold Change (Log2)
E
PanCK+KRT5+ in NP
PanCK+KRT5+ in CP
DDX3Y
RPS4Y1
KLF10
JUN
ZFP36
ATP5MC2
TMX3
PRKRIP1
FOS
TOP2A
UPK3BL1
TEX13B
EIF1AY
ATF3
AGR2
FDFT1
TMEM106C
SFRP2
PSCA
ERN2
KDM5D
ADIRF
UPK1B
ADRB1
RARRES1
H3C3
CYP3A5
TSPY1
SUPT7L
GABRP
Significance (−Log10)
Fold Change (Log2)
F
logFC
2.25 2.50 2.75 3
GO Terms
Cytoskeleton
Differentiation
Migration
Secretory/Extracellular
Immune Response
Cell Adhesion
Regulation of Proliferation
Plasma Membrane
Transcriptional Regulation
Reponse to Hypoxia

Figure 2

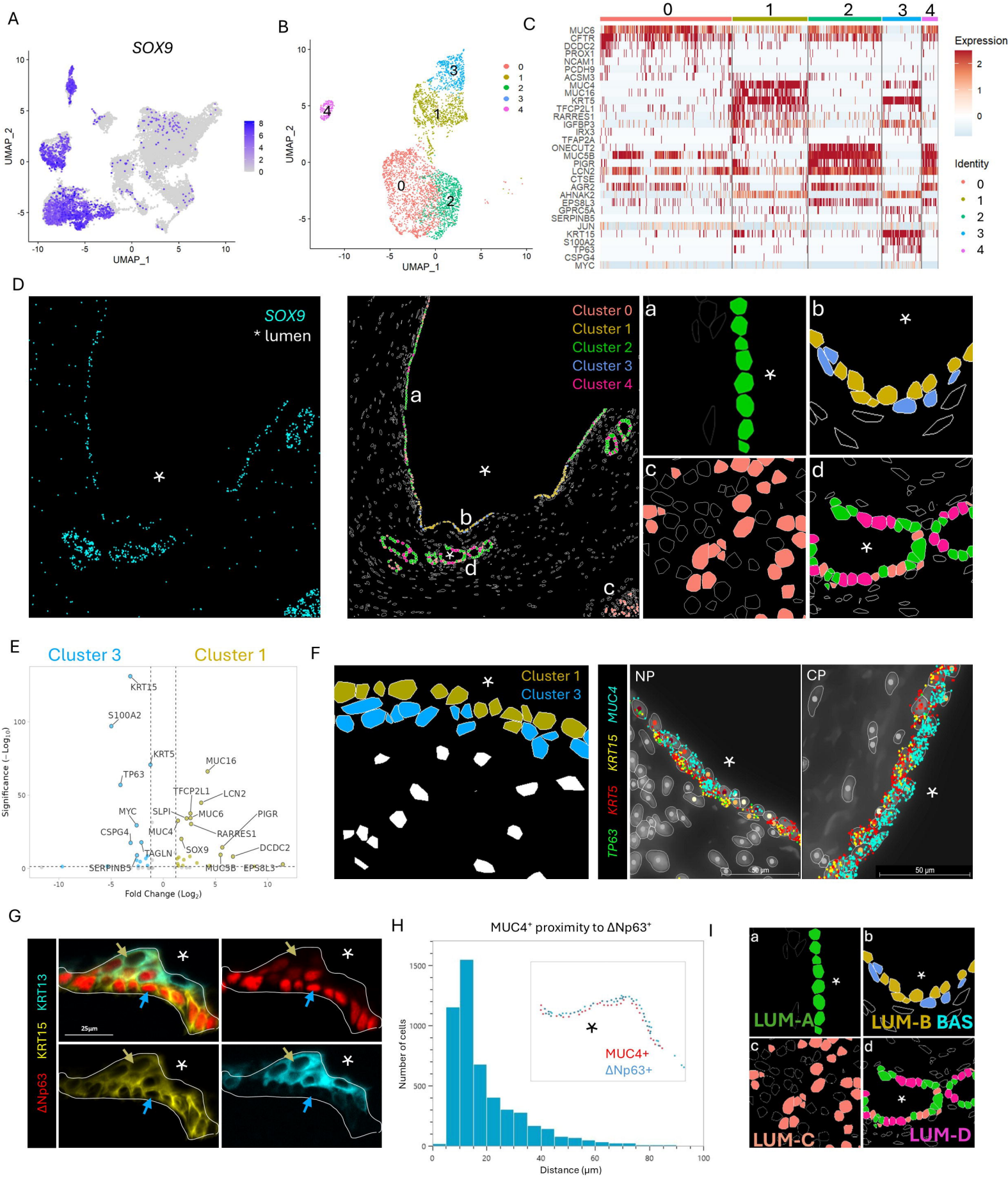
A
SOX9
UMAP_1
UMAP_2
B
0
1
2
3
4
C
Expression
Identity
MUC6
CFTR
DCDC2
PROX1
NCAM1
PCDH9
ACSM3
MUC4
MUC16
KRT5
TFCP2L1
RARRES1
IGFBP3
IRX3
TFAP2A
ONECUT2
MUC5B
PIGR
LCN2
CTSE
AGR2
AHNAK2
EPS8L3
GPRC5A
SERPINB5
JUN
KRT15
S100A2
TP63
CSPG4
MYC
D
SOX9
* lumen
Cluster 0
Cluster 1
Cluster 2
Cluster 3
Cluster 4
E
Cluster 3
Cluster 1
Significance (−Log10)
Fold Change (Log2)
KRT15
S100A2
KRT5
MUC16
TP63
TFCP2L1
LCN2
MYC
SLPI
MUC6
PIGR
CSPG4
MUC4
RARRES1
TAGLN
SOX9
DCDC2
SERPINB5
MUC5B
EPS8L3
F
Cluster 1
Cluster 3
MUC4
KRT15
KRT5
TP63
NP
CP
50 µm
G
KRT13
KRT15
ΔNp63
25µm
H
MUC4⁺ proximity to ΔNp63⁺
Number of cells
Distance (µm)
MUC4+
ΔNp63+
I
LUM-A
LUM-B BAS
LUM-C
LUM-D

Figure 3

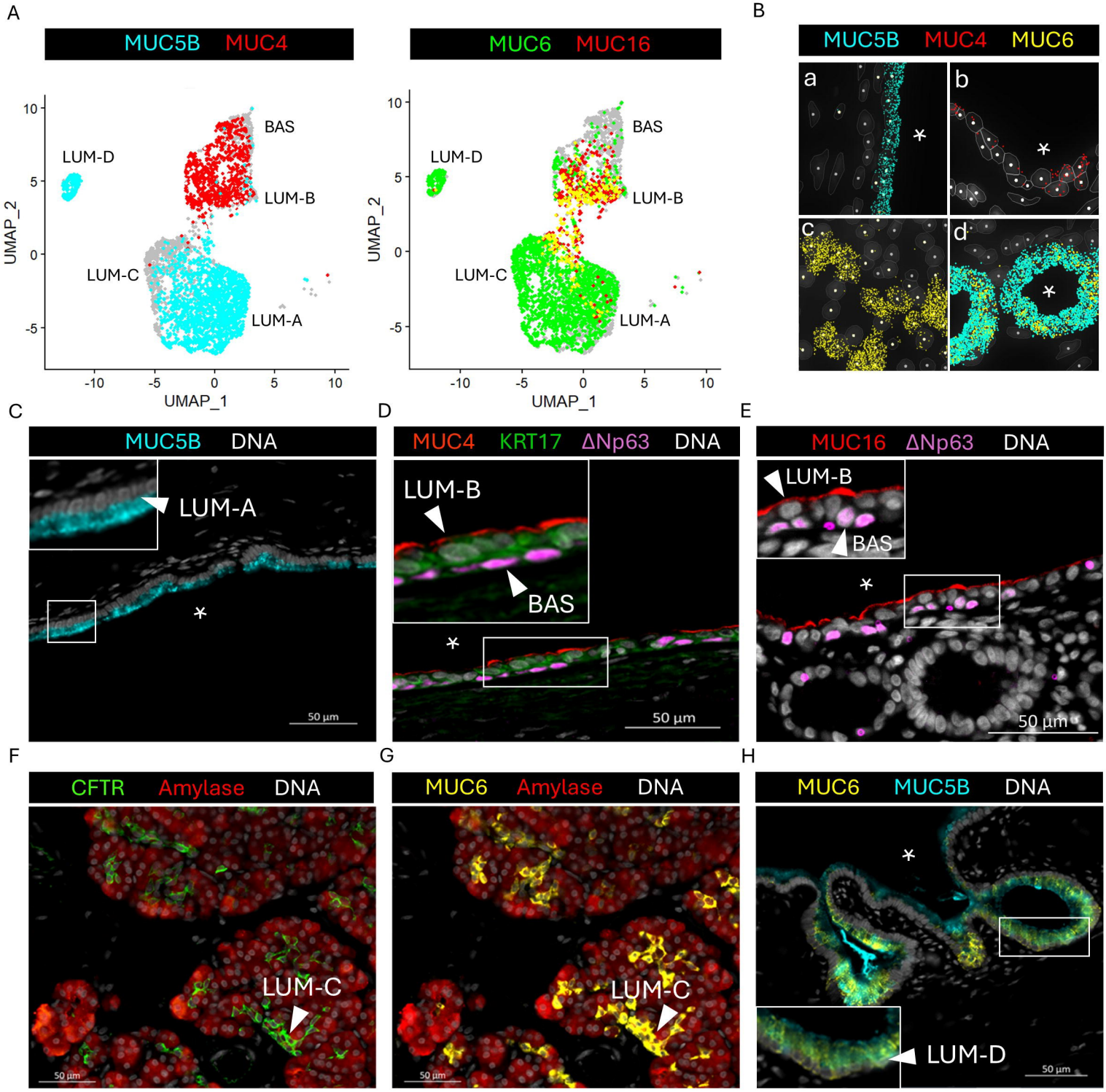

I

	LUM-A	LUM-B	LUM-C	LUM-D	BAS
MUC5B	●	○	○	●	○
MUC4	○	●	○	○	○
MUC16	○	●	○	○	○
MUC6	◑	◑	●	●	○
Location	Intralobular duct Interlobular duct Main pancreatic duct	Suprabasal	Intercalated duct	Pancreatic ductal gland	On basal lamina
Other markers	***LCN2***, *ONECUT2*	***KRT5***	***CFTR***, *DCDC2, PROX1*		***TP63, KRT15, S100A2***

● Expressed
○ Not expressed
◑ Expressed in subpopulation
Bold = confirmed at protein level

Figure 4

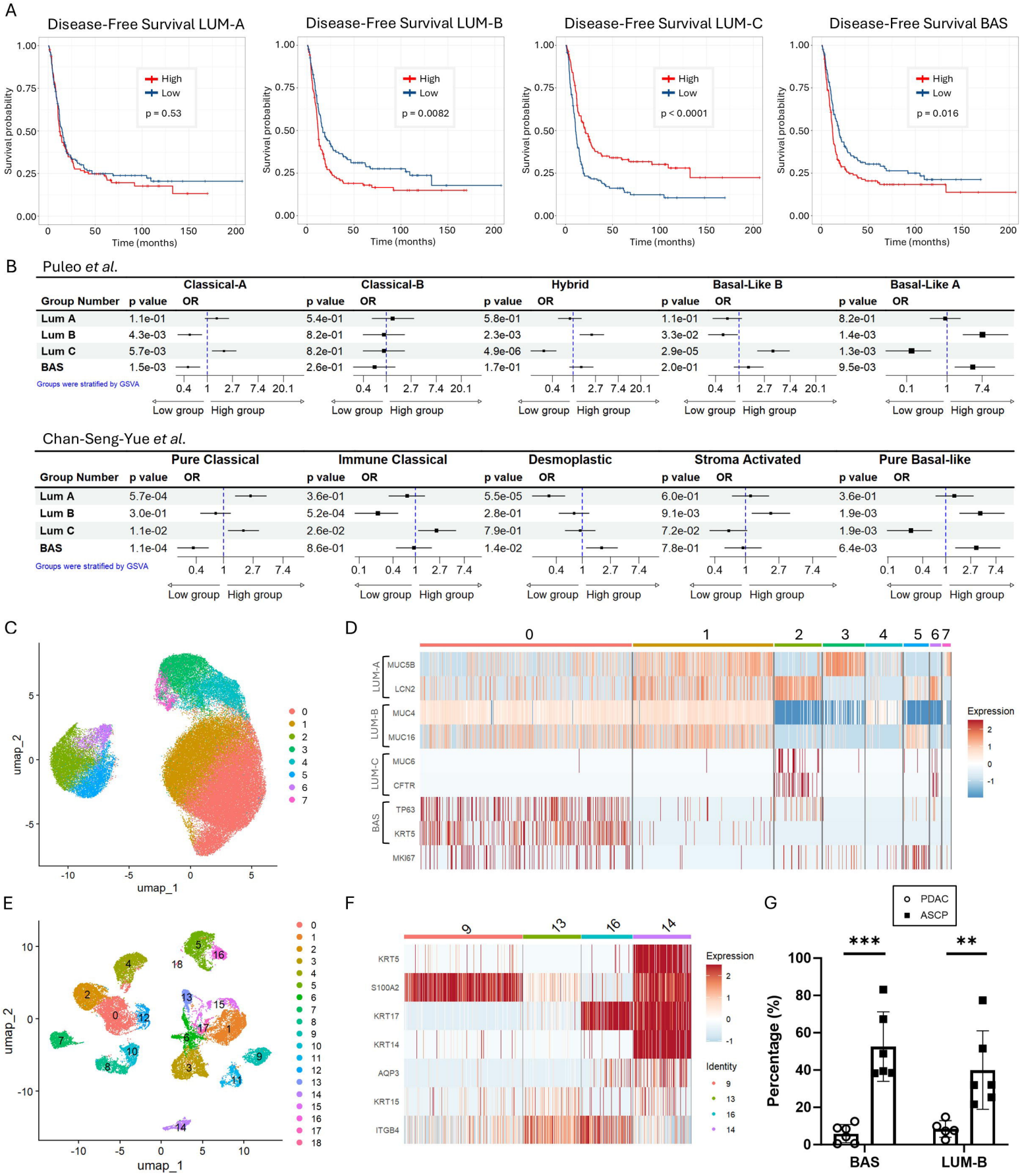
A
Disease-Free Survival LUM-A
Disease-Free Survival LUM-B
Disease-Free Survival LUM-C
Disease-Free Survival BAS
High
Low
p = 0.53
p = 0.0082
p < 0.0001
p = 0.016
Survival probability
Time (months)
B
Puleo et al.
Classical-A
Classical-B
Hybrid
Basal-Like B
Basal-Like A
Group Number
p value
OR
Lum A
Lum B
Lum C
BAS
Groups were stratified by GSVA
Low group
High group
Chan-Seng-Yue et al.
Pure Classical
Immune Classical
Desmoplastic
Stroma Activated
Pure Basal-like
C
umap_1
umap_2
D
MUC5B
LCN2
MUC4
MUC16
MUC6
CFTR
TP63
KRT5
MKI67
LUM-A
LUM-B
LUM-C
BAS
Expression
E
F
S100A2
KRT17
KRT14
AQP3
KRT15
ITGB4
Identity
G
PDAC
ASCP
Percentage (%)
BAS
LUM-B
H
ASCP
PDAC
ΔNp63 KRT5
KRT5
ΔNp63
100µm
100 µm

Figure 5

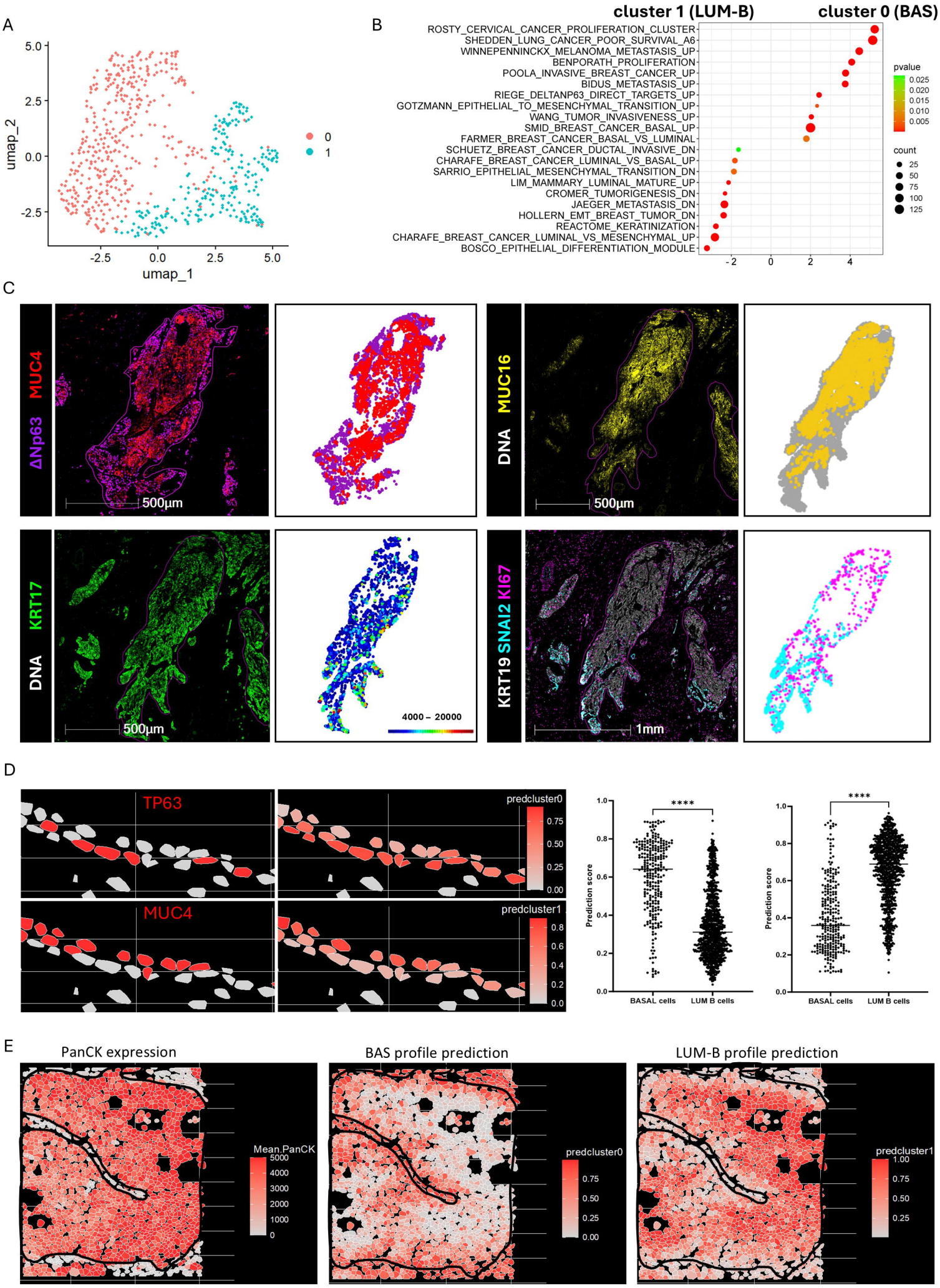
A
umap_2
umap_1
0
1
B
cluster 1 (LUM-B)
cluster 0 (BAS)
ROSTY_CERVICAL_CANCER_PROLIFERATION_CLUSTER
SHEDDEN_LUNG_CANCER_POOR_SURVIVAL_A6
WINNEPENNINCKX_MELANOMA_METASTASIS_UP
BENPORATH_PROLIFERATION
POOLA_INVASIVE_BREAST_CANCER_UP
BIDUS_METASTASIS_UP
RIEGE_DELTANP63_DIRECT_TARGETS_UP
GOTZMANN_EPITHELIAL_TO_MESENCHYMAL_TRANSITION_UP
WANG_TUMOR_INVASIVENESS_UP
SMID_BREAST_CANCER_BASAL_UP
FARMER_BREAST_CANCER_BASAL_VS_LUMINAL
SCHUETZ_BREAST_CANCER_DUCTAL_INVASIVE_DN
CHARAFE_BREAST_CANCER_LUMINAL_VS_BASAL_UP
SARRIO_EPITHELIAL_MESENCHYMAL_TRANSITION_DN
LIM_MAMMARY_LUMINAL_MATURE_UP
CROMER_TUMORIGENESIS_DN
JAEGER_METASTASIS_DN
HOLLERN_EMT_BREAST_TUMOR_DN
REACTOME_KERATINIZATION
CHARAFE_BREAST_CANCER_LUMINAL_VS_MESENCHYMAL_UP
BOSCO_EPITHELIAL_DIFFERENTIATION_MODULE
pvalue
count
C
ΔNp63 MUC4
500µm
DNA MUC16
500µm
DNA KRT17
500µm
4000 – 20000
KRT19 SNAI2 KI67
1mm
D
TP63
MUC4
predcluster0
predcluster1
Prediction score
****
BASAL cells
LUM B cells
E
PanCK expression
Mean.PanCK
BAS profile prediction
predcluster0
LUM-B profile prediction
predcluster1

Figure 6

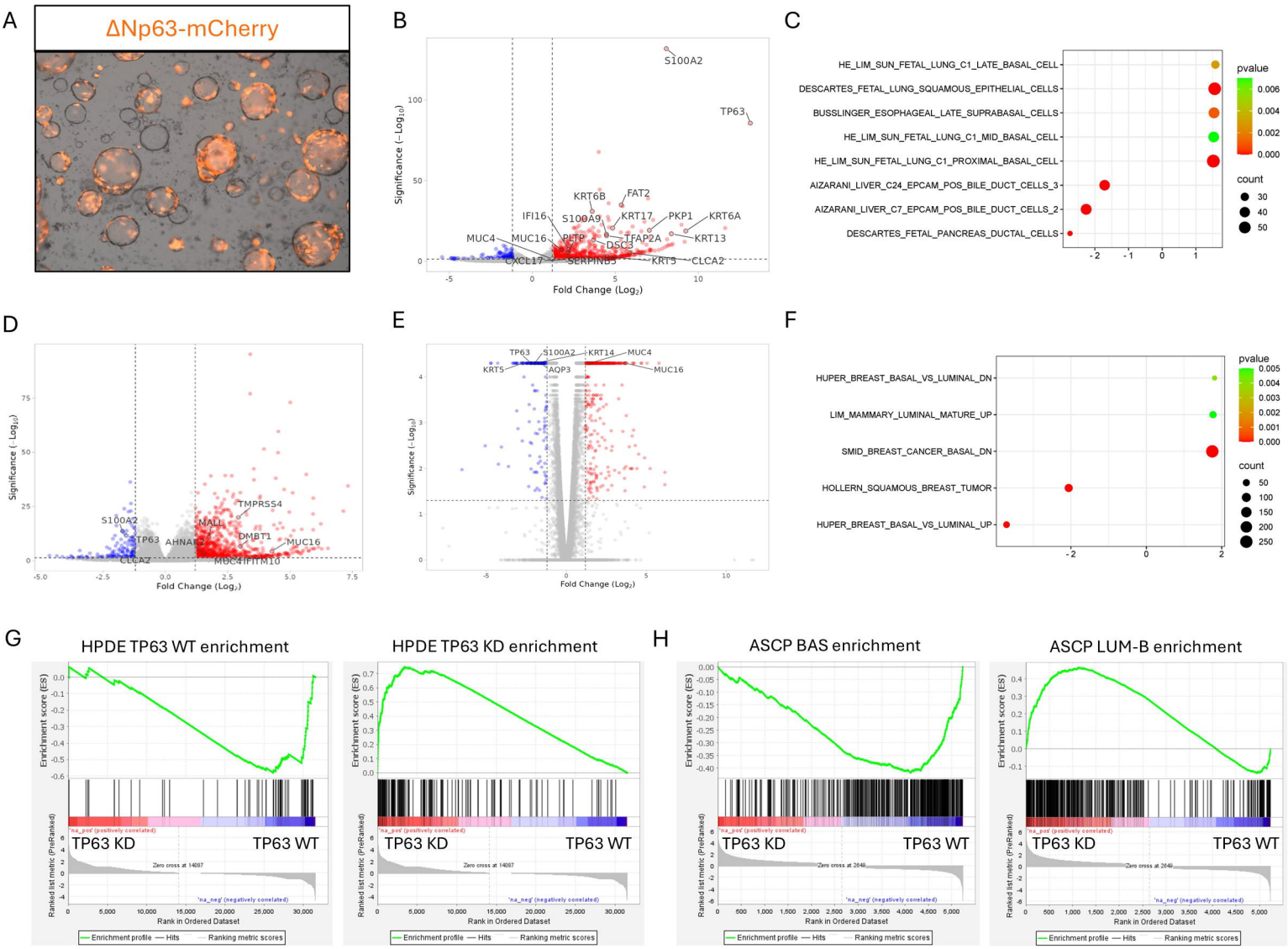

I

	Target	Therapy	Reference
BAS	UBE2S	Cephalomannine	(53)
	ITGB4	Specific antibodies / Dendritic cell vaccine	(54)
	TOP2A	Dactinomycin, norfloxacin, cryptolepine, doxorubicin, etoposide, mitoxantrone	(55-57)
	PTTG1	Dabrafenib	(58)
LUM-B	S100P	Cromoglycic acid	(56)
	ACSL1	Triacsin C	(59)
	NUPR1	Trifluorazine-derived compound (ZZW-115)	(60)
	TMPRSS4	Camostat mesylate	(61)
	LYPD3	Antibody-drug conjugate (BAY1129980), antibodies (Lupartumab, GT-002)	(62)
	PSCA	CAR-T therapy (PSCA-CAR)	(63)
	S100A9	Tasquinimod, paquinimod, viral nanoparticle vaccine	(56)(64-65)
	MUC4	Bosutinib, canertinib, guggulsterone, thymoquinone, Graviola extract, afatinib	(66)